Journal of Materials Chemistry B

Accepted Manuscript

ROYAL SOCIETY OF CHEMISTRY

www.rsc.org/materialsB

Graphical Abstract

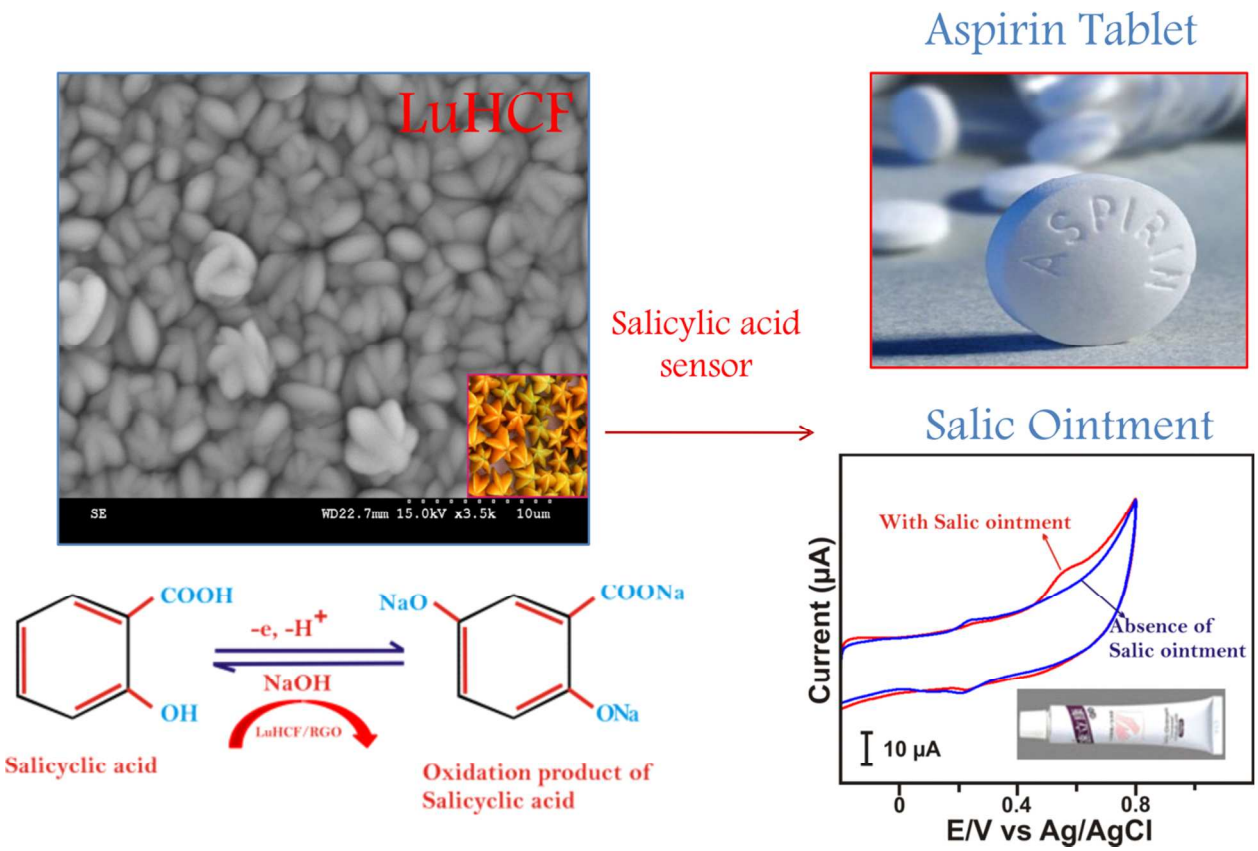

Controlled Electrochemical synthesis of new rare earth metal Lutetium hexacyanoferrate on reduced graphene oxide towards salicylic acid sensor.

Journal Name

RSCPublishing

ARTICLE

Controlled Electrochemical synthesis of new rare earth metal Lutetium hexacyanoferrate on reduced graphene oxide and its application to Salicylic acid sensor†

Cite this: DOI: 10.1039/xoxxoooooox

Received ooth January 2012,
Accepted ooth January 2012

DOI: 10.1039/xoxxoooooox

www.rsc.org/

Balamurugan Devadas‡, Rajesh Madhu‡, Shen-Ming Chen* Huai-Tse Yeh

Received (in XXX, XXX) Xth XXXXXXXXX 20XX, Accepted Xth XXXXXXXXX 20XX
DOI: 10.1039/b000000x

The hexangular star building-like Lutetium hexacyanoferrate (LuHCF) structure with an average size of ca. 8.0 ± 0.5 µm are synthesized by using a simple one-step electrochemical method, and highly dispersed on the reduced graphene oxide (RGO) modified glassy carbon electrode (GCE) support for the first time. The size and shapes of the as-synthesized LuHCF micro stars were controlled by deposition time. The LuHCF/RGO samples were characterized by a variety of analytical and spectroscopy techniques, *viz.* Scanning electron microscopy (SEM), Infra-red spectroscopy (IR), and energy dispersive X-ray spectroscopy (EDS), X-ray diffraction (XRD), and X-ray photoelectron spectroscopy (XPS). In addition, LuHCF/RGO/GCE was adopted for a novel electrochemical detection of salicylic acid (SA) using the cyclic voltammetry (CV) and amperomety methods. The charge transfer resistant value of LuHCF/RGO/GCE has smaller than LuHCF and bare GCE, which exhibits a remarkable electrocatalytic performance towards SA. Notably, SA sensor was found to exhibit a lower detection limit and high sensitivity of the SA sensor ca. 0.49 µM and 77.2 µA $mM^{-1}cm^{-2}$ respectively. The reported sensor possesses an excellent real time application with commercially purchased aspirin tablets and salic ointment. The excellent analytical parameters of the reported sensor, surpassing the reported modified electrodes, rendering practical industrial applications.

Introduction

Salicylic acid (SA) is a kind of phenolic acid and also known as 2-hydroxybenzoic acid. SA has been found in plants, and place a significant role in the development of plant growth, photosynthesis, and transpiration etc. However, the treatment of SA has grateful consideration toward the synthesis of pathogenesis-related proteins and alfalfa mosaic virus infected plants.[1] Owing to its unique properties such as keratolytic, bacteriostatic, fungicidal, and photo protective, thus, beneficial for wide range applications namely topical use, dermatologic conditions, reducing the rate of keratinocyte proliferation.[2] Moreover, SA has great contribution to heal several skin problems such as acne, hyperpigmentation, oily skin, large pores, and surface roughness.[3] Therefore, SA has been

*Department of Chemical Engineering and Biotechnology, National Taipei University of Technology, Taipei 10608, Taiwan. E-mail: smchen78@ms15.hinet.net
‡These authors contributed equally

widely used in the preparation of cosmetics and ointment due its peeling and flexible nature.[4] Hence, the effective and sensitive determination of SA is very important in pharmaceuticals and other cosmetic industries.

Owing to the numerous activities of pharmaceutical analysis, it is highly significant to develop sensitive and selective sensing systems for the detection of SA. Aforetime, P. Trinder et al., was reported for the determination Salicylate in biological fluid using ferric salt at spectrophotometer.[5] Nevertheless, there have been several reports on the detection of SA using different techniques including spectrophotometry,[6] Raman spectroscopy,[7] ultraviolet spectrometry,[8] gas Chromatography–mass spectrometry (GC-MS),[9] colorimetric technique,[10] liquid chromatography–tandem mass spectrometry,[11,12] and gas-liquid chromatography[13]. Aforementioned methods are disadvantage of high cost, need of expensive instruments and technical operators. In contrast to these methods, electrochemical techniques are more convenient, cost effective and easy to operate. However, there is a scanty reports on using the electrochemical method for SA detection sensor.[14, 15] Interestingly, we developed a simple and convenient amperometric method for the electrochemical determination of SA.

On the other hand, progress on new material using electrochemical technique is still challenging task for the many researchers. In spite of overwhelming activies on metal hexacyanoferrate, rare earth Metal-HCFs have been also widely used in electrochemical sensor applications.[16-20] So far several rare earth Metal-HCF such as dysprosium,[21,22] samarium,[23,24] and lanthanum HCF[25] respectively have been reported for preparation and characterization. Nonetheless, kind of rare earth Metal-HCFs having of fascinating morphologies, flower and Christmas tree-like CeHCF,[26] diamond like NdHCF,[27] LaHCF,[28] and Carambolalike HoHCF.[29] Moreover we have demonstrated microstar like DyHCF and flower like YHCF for sensor application in our recipe reports elsewhere.[30,31] Among them, in the order of rare earth metal, lutetium is one of the significant material for electrochemical sensor application.[32] In recent decades, electrochemical properties and the applications of lutetium phthalocyanines have been also investigated.[33-36] Besides, reduced graphene oxide (RGO) is an inspiring material due to its unique properties such as electrical, thermal and mechanical properties, and it can be used as efficient substrate material. Hence, RGO modified electrode has been widely used for biofuel cells, energy storage devices and biosensor applications.[37-41] Moreover, RGO is more favorable to prevent the uncontrollable growth of the MHCF, hence, favorable for catalytic reactions.[42,43] Contrast to the earlier reports on electrochemical methods by Jiang et al., and M. A. Raj et al., the reported electrochemical reduction of GO was performed with 0.1M KCl solution containing metal and ferricyanide solution. Moreover, only 10 consecutive CV cycles were scanned for electrochemical reduction.[44,45]. Interestingly RGO can retain the electrochemical behaviour of hexacyano ferrate (HCF) film and enhaces the electron transfer ability betweern HCF and GCE. Hence composites of graphene with HCF composite has prevalent consideration for different applications[46,47] Owing to dintinctive properties of RGO-HCF has received greatful attention for electrocatalysis applications in recent years[48,49,31]. To the best of our knowledge with an extensive literature survey, there is no report for the LuHCF/RGO hybrid material. Hence, the electrochemical, structural and morphological characterisation, and wide applications of LuHCF are still intriguing statement. Therefore, in this work we developed an amperometric method for the electrochemical preparation of LuHCF for the first time.

Herein, we demonstrate a novel electrochemical route for the preparation of LuHCF/RGO composite material for the SA sensor. The LuHCF micro star particle structure was attained by controlling the deposition time. The as-synthesised LuHCF/RGO composite material was characterized by using analytical and spectroscopy techniques. The determination of SA was carried out by amperometric method, and the real time application of reported sensor was performed with Aspirin tablets and Salic ointment samples.

2. Experimental Section

2.1 Materials and method

Lutetium (iii) chloride hexahydrate was obtained from sigma Aldrich. $K_3Fe(CN)_6$ and KCl were purchased from Wako pure chemical industries, Ltd. Salicylic acid was purchased from Yakuri Chemicals.CO.LTD. Sodium hydroxide was purchased from sigma Aldrich. All other chemicals were purchased of analytical grade and used as received. Supporting electrolyte 0.1M KCl and all the reagents were prepared by doubly deionized distilled water. Prior to electrochemical experiments, pure nitrogen gas was purged through the experimental solution.

The entire electrochemical measurements were carried out using CHI 1205A work station using three electrode system of glassy carbon electrode as working electrode, Ag/AgCl as reference electrode and Pt wire as counter electrode in an electrochemical cell. The electrochemical cell having. Amperometric studies were carried out using rotating ring disk electrode (RRDE-3A), BAS instrument made in Japan. The morphological studies were carried out using Hitachi S-3000 H scanning electron microscope (SEM). Energy dispersive X-ray (EDX) spectra was recorded with HORIBA EMAX X-ACT.

2.2 Synthesis of Graphene oxide

Graphene oxide (GO) has synthesized by the hummer's method. Briefly, the graphite oxide was synthesized by treatment of raw graphite using sodium nitrate and potassium permanganate in ice bath. Then followed by the addition of 3% hydrogen peroxide to reduce the permanganate and manganese dioxide. The obtained brownish graphite oxide was washed with warm water, and finally the graphite oxide was collected by centrifugation. Further, graphite oxide was dispersed in water in the ratio of 1mg/ml using sonication to get GO solution.

2.3 Fabrication of modified electrode

Prior to the fabrication of electrode, the GCE was well polished with alumina powder, ethanol and DD water and dried in air atmosphere and 5 µl of the as-synthesized GO was drop casted on GCE surface and dried. The GO modified GCE was placed in a supporting electrolyte KCl solution containing equal amount of $LuCl_3$. $6H_2O$ and $K_3Fe(CN)_6$. Then 10 consecutive CV scans were performed at GO/GCE, and the amperometric deposition was performed on the same solution with a constant applied potential of -0.2 V for 500 Sec.

3. Result and Discussions

3.1 Amperometric deposition of LuHCF on RGO/GCE

Fig. 1 depicts the 10 consecutive CV cycles of the electrochemical reduction of GO. As shown in Fig. 1, in first cycle a large cathodic peak appears at -1.0V attributed to the reduction of oxygen functionalities on GO. Meanwhile the GO film was stabilized with ferricyanide solution, and RGO/GCE was turned back to the amperometric deposition of LuHCF. At constant potential of -0.2V, the amperometric scan was performed for 500 Sec. The positively charged Lu^{3+} ions are consequently adsorbed the negatively charged hexaycanoferrate (HCF) particles, which formed as LuHCF particles. Here GO has been act as a substrate material for efficient deposition of LuHCF. Based on a previously reported mechanism, the formation of LuHCF particles can be expressed in equation 1.

$$Fe(CN)_6^{4-} + Lu^{3+} + K^{+} + H_2O \rightarrow KLu[Fe(CN)_6].H_2O \quad \text{---------} \quad (1)$$

Scheme 1 represented the mechanism of nucleation and growth of LuHCF on RGO at different deposition time. To provide clear insights into the mechanism of formation of the LuHCF particles, we monitored the nucleation and the growth of the particles formed at different deposition times through amperometry. As shown in scheme 1, distorted spherical shaped particles with sizes (1.5±2µm) were formed on the surfaces of RGO at 100 s.The growth of petals occurred from the adjacent facets of the particles. At 300 s, increased nucleation of the particles from the side facets occurred on the surfaces of the RGO, leading to the formation of gooseberry shaped particles with sizes two times that had star shaped petals. When the deposition time was increased to 500 s, the nucleation of the particles at the adjacent star shaped petals increased greatly, resulting in the formation of well-defined petals that are separated through defined edges. The as-formed particles resembled that of hexangular star-fruit shaped particles. It has to be noted that deposition time played a key role in controlling the nucleation of the particles and the shape of the petals and the morphology of the particles[50].

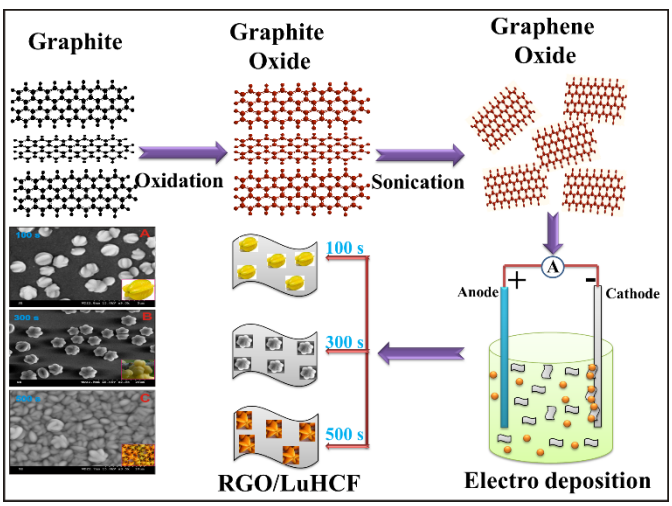

Scheme 1: Electrochemical growth and nucleation mechanism of LuHCF on RGO.

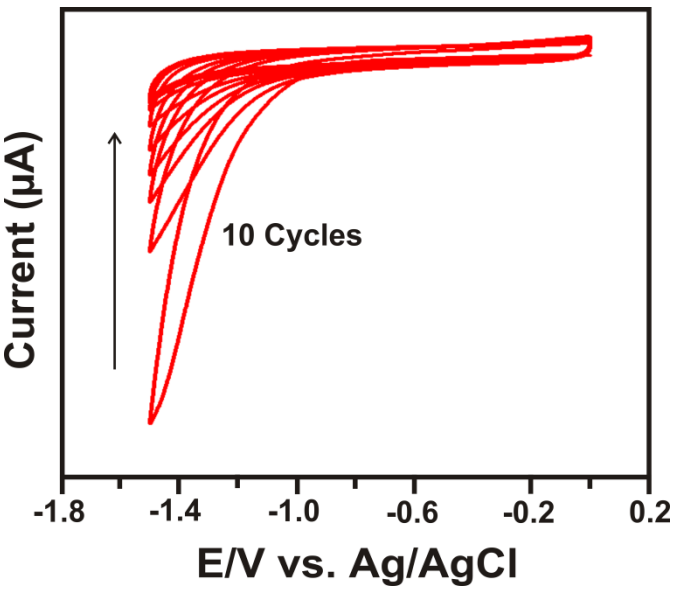

Fig. 1 CVs of electrochemical reduction of graphene oxide (GO) in 0.1M KCl containing 5 mM of $K_3Fe(CN)_6$ and $LuCl_3.6H_2O$ at scan rate of 50 mV/s.

3.2 Characterization of RGO

The FT-IR spectroscopy of GO and RGO was exhibited in Fig 2A . It can be seen that the oxygen functionalities groups such as –OH, epoxy, -C=O and - C-O in the spectrum of GO. The high intensity peak at 3400 cm-1 validating the presence of stretching vibration of υ(–OH) group present in GO. The sharp peak at 1720 cm-1attributed to υ (–C=O) and 1619 cm-1 corresponding to υ (-C=C) groups were present in GO. The intensity at 1068 cm-1 indicating υ (– C–O) groups of GO. All these peak intensities ascribed to stretching vibrations of oxygen functionalities of GO. Whereas, significant peaks were decreased, indicating reduction of oxygen functionalities in GO. Besides UV-Vis spectroscopy of as synthesized GO and RGO were demonstrated in Fig 2B. As shown in UV-Vis spectrum a broad absorption peak at 230 nm corresponding to π - π* transition and shoulder peak at 295 nm for n – π* transition was observed for GO (black colour). The spectrum of RGO was exhibited in red colour. The π-π* transition peak was red shifted to 265 nm indicating reduction of oxygen functionalities on GO surface and rearrangement of the electron conjugation structure.[51]

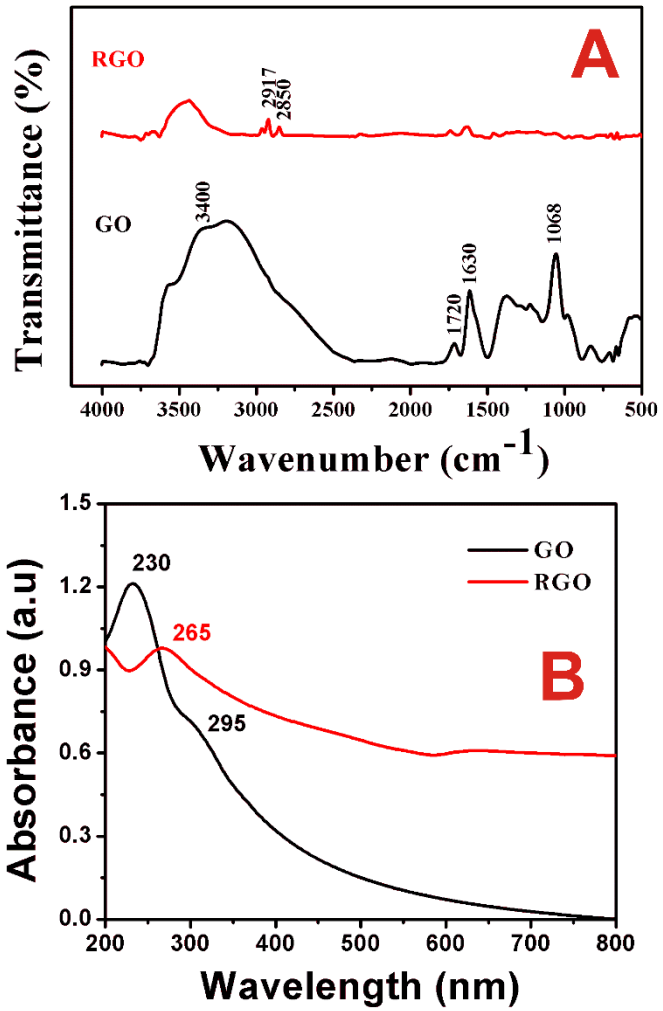

Figure 2: A FT-IR and B) UV-Vis spectroscopy of GO and RGO.

3.3 Structural and morphological studies of LuHCF

The morphological studies of rare earth LuHCF particle is very interesting to discern the size and shape of concerned particle. Fig. 3 elucidate the different morphologies of LuHCF particles. The deposition of LuHCF micro particle has been monitored at different interval time of amperometric deposition. As shown in Fig. 3A, the star fruit like structure formed at 100 Sec. The each particle having equal size of ±1.5-2 μm. Further, the particles became gooseberry like structure and the size of micro stars were increased two times at 300 Sec. as shown in Fig. 3B. Upon increasing the deposition time at 500 Sec, we obtained the closely packed star like structure of LuHCF (Fig. 3C). Every star like a particle having a diameter size of 8.0 ± 0.5 μm and deposited on the electrode surface uniformly displayed in Fig. 2D. The Fig 3 E and F shows the LuHCF deposited

on GCE and RGO surface. It can be seen that LuHCF highly distributed on RGO similar like with GCE.

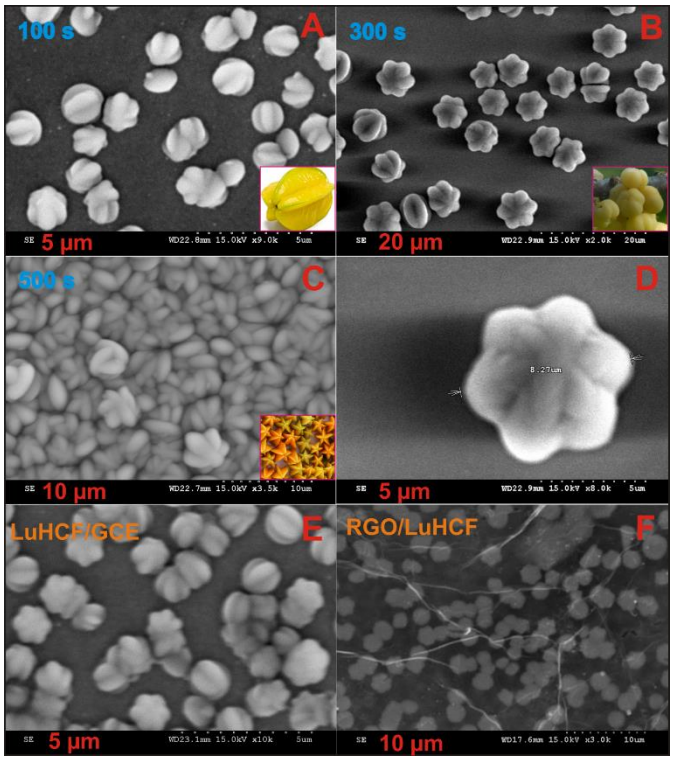

Fig. 3 SEM of LuHCF at different deposition time A) 100 Sec B) 300 Sec C) 500 Sec and D) single particle image of LuHCF. E) LuHCF on GCE and F) LuHCF on RGO surface.

3.4 Elemental analysis and FT-IR spectroscopy of LuHCF

Fig. 4A shows the EDX spectra of as-deposited LuHCF. As shown in the EDX graph, the corresponding elements of Carbon, Lutetium, Ferrous, nitrogen and potassium are present in the deposited LuHCF, and it reveals that the LuHCF having of significant weigt % of all elements. The EDX profile of a single LuHCF particle reveals the presence of 27 % of Carbon, 28 % of Lutetium, 15 % of potassium, 20 % of ferrous ion and 10 weight % nitrogen ion. Accordingly, the EDX result confirms the LuHCF complex formed efficiently. The FT-IR spectroscopy of as-synthesized LuHCF was displayed in Fig. 4B. According to Prussian blue (PB) and its analogues the corresponding peaks of LuHCF are located in Fig. 3B. The very sharp with high intensity peak was observed at 2080.9 cm^{-1}, validates the stretching vibration of ferricyanide (υ(CN)) C≡N present in LuHCF. The broad peak at 1597.93 cm^{-1} corresponding to the H-O-H bending mode of LuHCF complex. Moreover, the two broad peak at 2876 and 2973 assigned to the stretching vibration of two kind of water molecule.

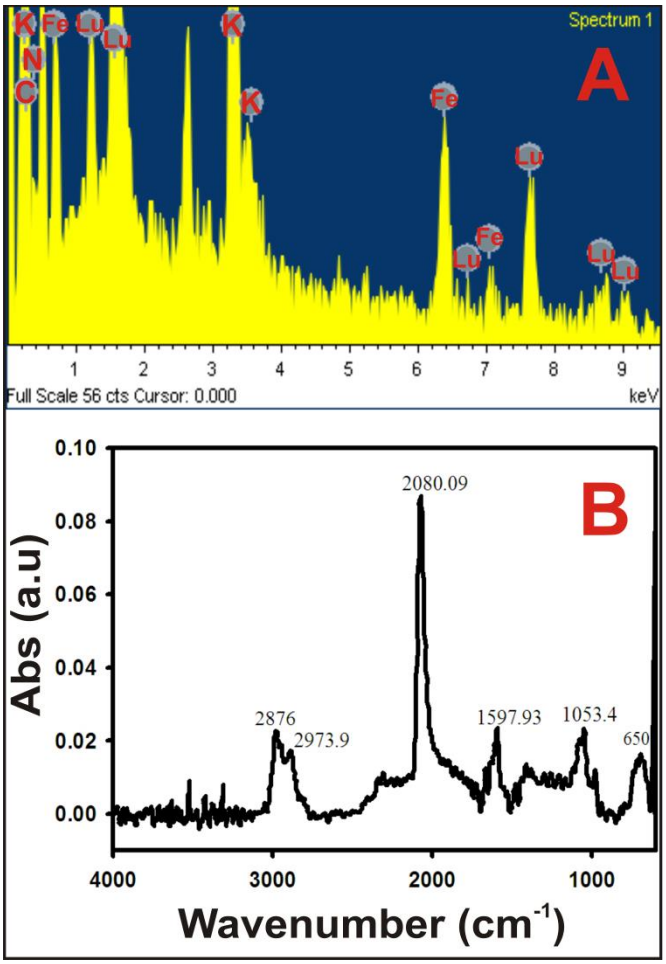

Fig. 4 A) EDX analysis and B) FT-IR spectroscopy of LuHCF.

3.5 XRD and XPS analysis of LuHCF

Fig. 5A displays the XRD pattern of as-deposited LuHCF micro star particle. As shown in the XRD pattern the highest peak intensity of the LuHCF was descried and mentioned for corresponding hkl value. Moreover, there is no literature available for $KLu[Fe(CN)_6]$ complex and its characterizations. Nevertheless, properties and high intensity XRD peaks of LuHCF was similar with the rare earth metal hexacyanoferrate. The high intensity peaks at 15.5°, 19.2° and 24.5° were common for all lanthanide metals based on the previous report [52] (black colour). The broad diffraction peak of RGO was appeared at 28° indicating LuHCF micros stars were distributed throughout the RGO sheets (Red color) . All the peaks were referred according to JCPDS cards. The referred JCPDS card numbers were JCPDS # 01-072-4771, JCPDS # 00-047-1329,

JCPDS # 00-046-1089 and JCPDS # 01-071-8282. The presence of all peak intensities according to JCPDS cards suggesting orthorhombic (Cmcm space group) structure model of LuHCF complex. When compare to the other rare earth metal hexacyanoferrate complexes, the structure model are similar with orthorhombic structure of LuHCF.[19,30,31,53] Furthermore, X-ray photoelectron spectroscopy (XPS) is known to analyze the chemical composition and the binding energy. Fig. 5B shows the XPS survey spectra of LuHCF, which exhibits the corresponding peaks appeared for FeS_3 $(CN)_3$, Fe 3s, Cl 2p, K 2p3/2 (chloride), and O1s which is consistent with the obtained EDS results.[54-56]

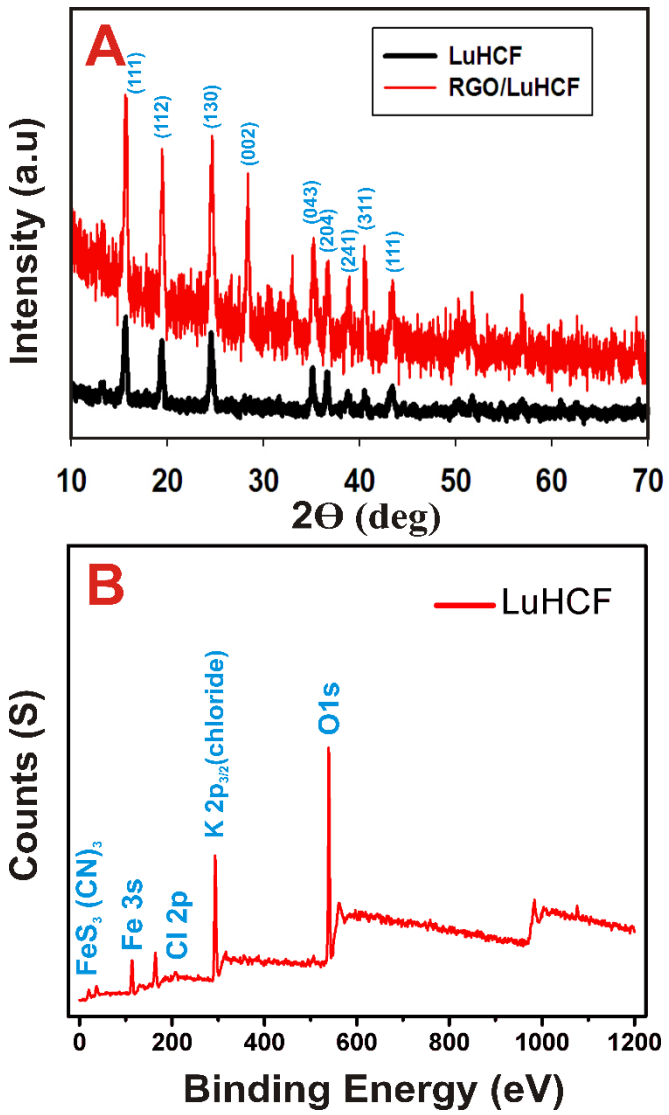

Fig. 5 A) XRD pattern and B) XPS survey spectra of LuHCF.

3.6 Cyclic voltammetric determination of SA

To evaluate the electrocatalytic activity of the various electrodes, cyclic voltammograms (CVs) were recorded for the a) LuHCF/RGO/GCE b) RGO/GCE c) LuHCF and d) bare GCE in 0.3M NaOH containing 1 mM of SA at a scan rate of 50mV/s. As shown in Fig. 6A, the well-defined SA oxidation peak initiation was observed on a) LuHCF/RGO/GCE at 0.45 V. Besides, other modified electrodes b) RGO/GCE c) LuHCF/GCE and d) bare GCE shows the very poor SA oxidation initiation peak at 0.55 V, 0.6 V and 0.65, respectively. It is noteworthy that the oxidation peak potential of LuHCF/RGO/GCE-modified electrode was 150 and 230 mV less positive potential than LuHCF modified and bare GCE. Moreover, oxidation peak current of SA at LuHCF/RGO/GCE was several times higher than that of other modified GCEs.

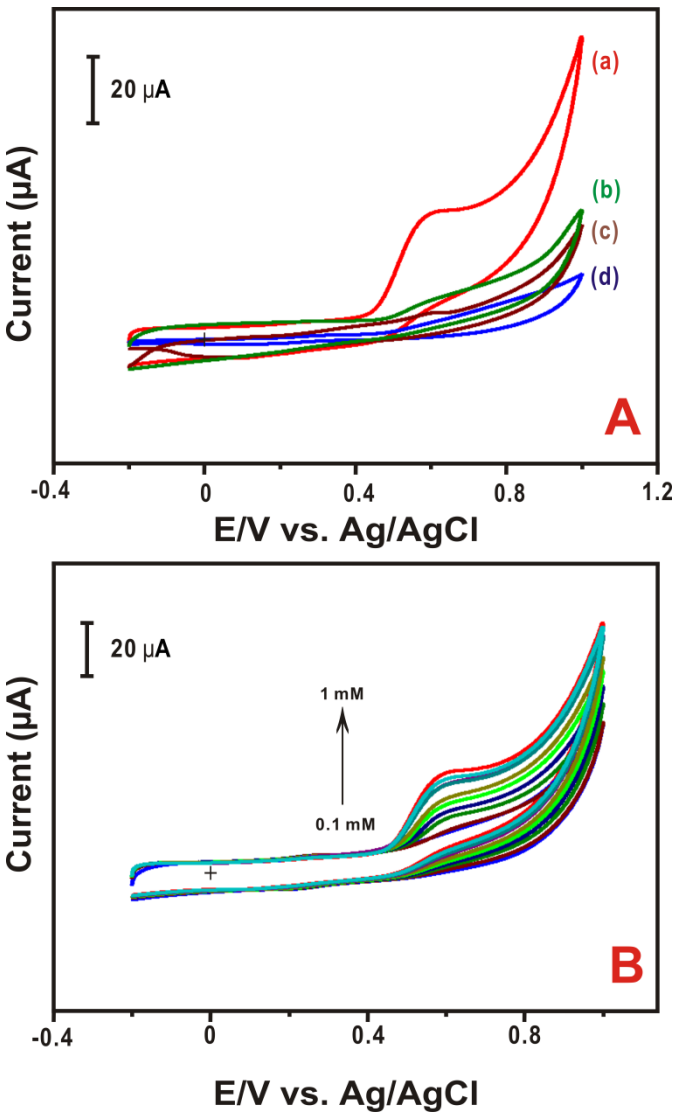

Fig. 6 A) CV of different modified film a) LuHCF/RGO/GCE b) RGO/GCE c) LuHCF and d) bare GCE in 0.3M NaOH containing 1

mM of SA at scan rate of 50mV/s. B) CV of LuHCF/RGO/GCE in 0.3M NaOH containing different concentration of SA at scan rate of 50 mV/s.

To assess the analytical performances of the proposed SA sensor, the LuHCF/RGO/GCE-modified GCE was performed by using CV measurement. The cyclic voltammetric electrochemical determination of SA was shown in Fig. 6B. It can be seen that the SA oxidation peak current at 0.5 V increased linearly with their increasing the concentrations of SA, meanwhile no reduction peak was observed attributed to the fast irreversible electrochemical reaction. In the first step the SA was adsorbed on LuHCF, caused to formation of phenoxy radical and further oxidized into phenoxy cation. Finally the carboxyl– hydroquinone was obtained as the product of this electrochemical reaction. Here the supporting electrolyte NaOH has been used for the efficient oxidation of SA. The SA oxidation mechanism can be expressed as shown in the scheme. 1.

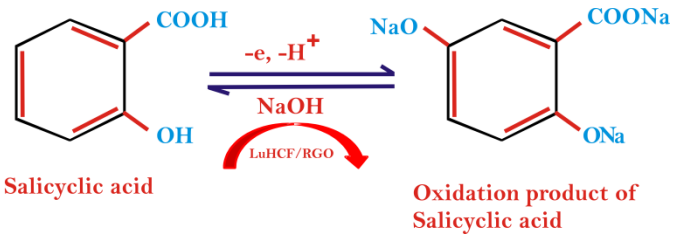

Scheme 2. Electro-oxidation process of Salicylic acid.

3.7 Electrochemical impedance spectroscopy

EIS has been employed for discerning the electron transfer behavior of the reported fabricated electrode. Fig. 7A shows the Nyquist plot of real component (Z_{re}) and imaginary component (Z_{im}). The inset figure represents the Randles circuit parameters (inset figure) corresponds to the charge transfer resistance (R_{ct}), solution resistance (R_s) and double layer capacity (C_{dl}) of the films. It can be seen that in Fig. 7A, bare GCE has the lower charge transfer resistant than LuHCF/GCE, RGO/GCE and LuHCF/RGO/GCE. Though the LuHCF and RGO modified GCE has lower semicircle value than bare GCE, comparatively higher charge electron transfer resistant than the fabricated LuHCF/RGO/GCE. Therefore, the reported modified GCE has the excellent electron transfer capacity than LuHCF, RGO modified and bare GCE.

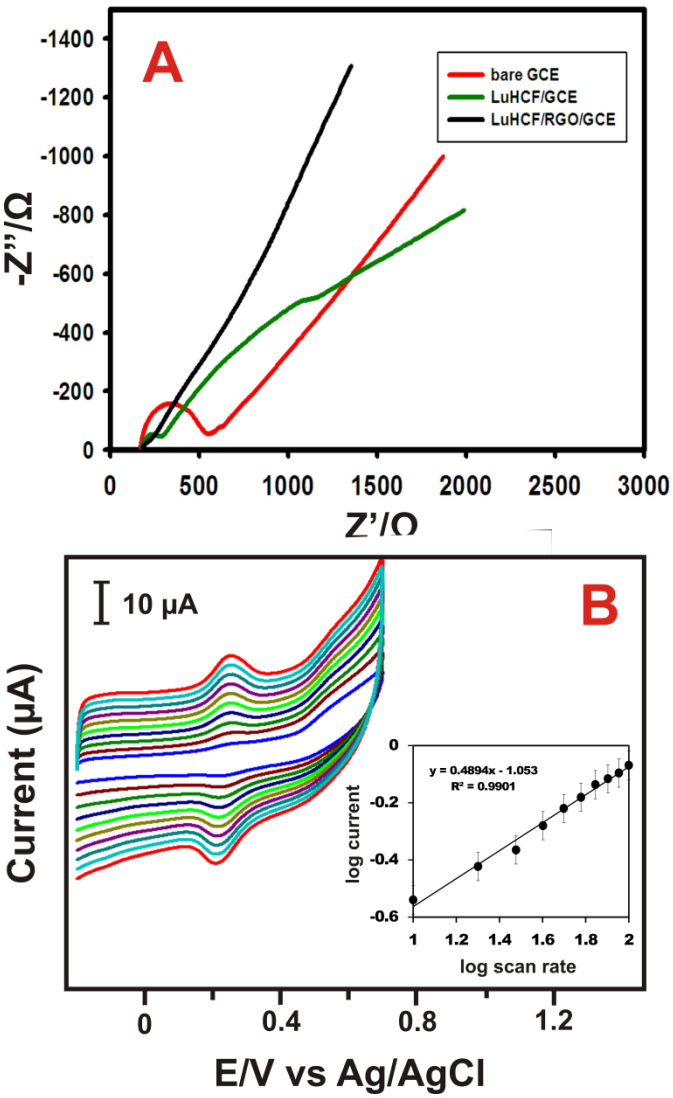

Fig. 7 A) EIS of different modified GCE bare, LuHCF and RGO/LuHCF B) CV of RGO/LuHCF modified GCE in 0.3M NaOH containing 100 µM of SA at Different scan rate (100 to 1000 mV/s).

3.8 Different scan rate

The CVs of RGO/LuHCF modified GCE in the presence of 100 µM of SA in 0.1M NaOH at different scan rate (10 to 100 mV/s) was shown in Fig. 7B. The linear increase of both redox peak at 0.2V corresponding to the LuHCF and SA oxidation peak around 0.4 V was observed when increasing the scan rates of 10 to 100 mV/s. The inset of Fig. 6B displays the calibration plot of log scan rate (log υ) *vs* log current (log I_{pa}). The linear regression equation of the calibration plot can be expressed as I_{pa} (µA) = 0.489 log *v* (mV/s) - 1.053, R^2 = 0.9901. As shown in the regression equation the value of scan rate was observed as 0.489 log υ, which is very near to the

theoretical value of 0.500, reveals that the electrochemical reaction occurred on the electrode surface was diffusion controlled process. Moreover the redox peak of LuHCF at 0.2 V was increased linearly with scan rate indicating a surface confined process.

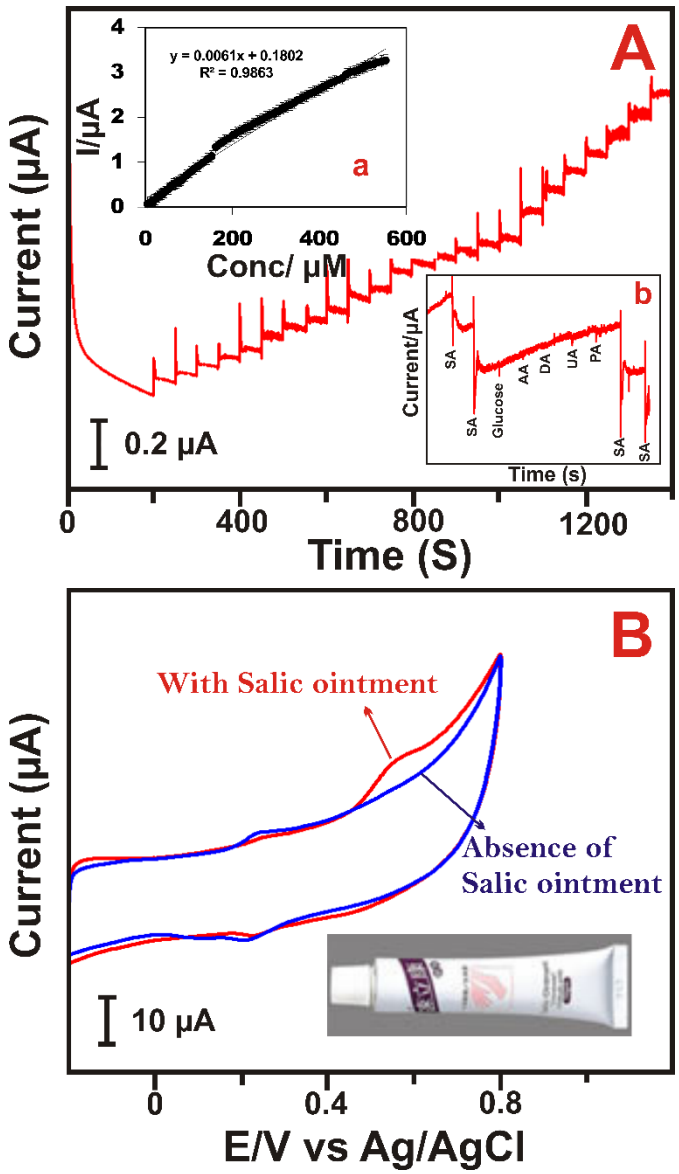

Fig. 8 A) Amperometric response of the LuHCF/RGO/GCE for the sequential addition of SA at applied potential (E_{app}) of +0.55 V. (Inset a) Calibration plot of Concentration Vs current b) amperometric response of interference compound. B) CV of LuHCF/RGO/GCE in Salic ointment (500 mg/10 ml).

3.9 Amperometric determination of SA

To further assess the analytical performances of the proposed SA sensor, electrocatalytic activities of the LuHCF/RGO-modified rotating ring disk electrode (RRDE) was evaluated by the amperometry method at an applied potential (E_{app}) of +0.55 V, as shown in Fig. 8A. At constant regular intervals (50s) 50µm of SA was injected while the RRDE (1500 RPM) rotates continuously into NaOH solution. The excellent and well sharp SA amperometric responses were observed within a 5 Sec. of every additions. The inset to Fig. 8A expressed the calibration plot of SA concentration *vs* current. It can be seen thatthe SA oxidation currents were linearly increased with increasing concentrations of SA. The linear regression equation can be expressed as, I = 0.0605 C (µM) + 0.1802, R^2 = 0.9863. The low limit of detection for the reported film modified GCE for SA sensor has been calculated using the formula of LOD = 3σ/S, where σ is the standard deviation of the three blank and S is the sensitivity. The calculated LOD and sensitivity of the SA sensor as 0.491 µM and 77.2 µA $mM^{-1}cm^{-2}$, respectively. The obtained analytical parameters is more feasible compared to various modified electrodes available in the literature (Table 1).

3.9.1 Selectivity

The selectivity of the reported sensor is extremely important for the practical applications. So we have performed the selectivity of SA sensor in the presence of some common coexisting interference compounds such as Ascorbic acid (AA), Dopamine (DA), Uric acid (UA), Glucose and Paracetamol (PA) using amperometric technique. The right bottom inset of Fig 8A shows the selectivity of the SA sensor at RGO/LuHCF modified GCE. As shown in inset Fig 8A, the well-defined amperogram responses were observed at each 100 µM of SA (a). But no remarkable response was observed for 100 µM each addition of b) Glucose. c) AA, d) DA, e) UA and f) PA. However, significant response was observed subsequent addition of SA, validating selectivity of reported sensor. Thus, SA could be determined selectively at RGO/LuHCF modified GCE without interference of coexisting species.

3.9.2 Real sample applications

To investigate the versatile application of the SA sensor for practical analysis of real samples, the fabricated GCE was tested with commercially available tablets (aspirin) and ointment (Salic ointment). The results are shown in Table 2 and Fig. 8B, respectively. The 3 aspirin tablets were weighed in analytical balance and crushed using a cleaned mortar, and prepared for the required concentration. The CV technique was employed for the tablet sample analysis. Three different concentration of samples

were analysed using LuHCF/RGO modified GCE at the same conditions. From the amount of added and found in tablet samples, the calculated recoveries are summarized in Table 2. It is found that satisfactory recovery rate exceeding ca. 99.7% for the 3 samples may be inferred for these real samples, indicating the promising perspective application of the proposed SA sensor for analysis of real samples.

Further, to widen the applications of the reported SA sensor, CV technique was employed for the determination of SA in Salic ointment. The 1 gram of Salic ointment contain standard salicylic acid of 25 mg. We squeeze out all Salic ointment into an empty bottle. Then 500 mg of ointment was weighed and dissolved in NaOH with use of stirring and ultra-sonication. The 500 mg/10 ml of ointment placed in an electrochemical and CV was recorded at LuHCF/RGO/GCE. As shown in Fig. 8B, the SA oxidation peak was observed at 0.55 V at the scan rate of 50 mV/s. It is noting that the reported modified GCE would be worthy to reach up the prototype level sensor for the determination of SA.

3.9.2 Repeatability, reproducibility and stability

The repeatability of the fabricated GCE for the reported SA sensor performed by additional CV measurements at same electrolyte conditions. The reported electrochemical sensor shows the good repeatability with below 5 % of relative standard deviation (RSD) for five successive measurements. Moreover, the reported sensor exhibits excellent reproducibility with an RSD 4.5% for five individual measurements. Besides, the storage stability of the LuHCF/RGO modified GCE was assessed by CV measurements in presence of 1 mM of SA in 0.3 M NaOH, and the oxidation peak currents were monitored periodically, and the fabricated GCE was maintained at air room temperature. The oxidation peak current of SA was stable for three consecutive days and the peak current retained with 95% for two weeks (not shown), indicating an excellent storage stability.

4. Conclusion

In summary, we report a simple and efficient electrochemical growth of a new rare earth metal LuHCF on RGO modified GCE for a novel electrochemical determination of SA with their practical catalytic applications. The LuHCF micro particles have shown different size and shapes of morphology respects to their controlled time of amperometric deposition. The novel SA sensor reported herein possesses a very lower detection limit, excellent durability, and high sensitivity over wide linear range of SA, better than the other reported modified electrodes. Moreover, we also proved that the SA sensor at LuHCF/RGO/GCE has ability to real time application with tablet and ointment samples respectively. The LuHCF/RGO/GCE also exhibited a remarkable performance for real time applications with tablet and ointment samples, rendering a large-scale production and wide industrial applications.

Acknowledgement

The authors are grateful to the financial supports from Ministry of Science and Technology. Taiwan (ROC). The authors thank Dr.Arun Prakash Periasamy and Dr. Thiagarajann Natarajan for helpful discussions.

References

1 R.A.M.H.V. Huijsduijnen, S.W. Alblas, R.H.D. Rijk and J.F. Bol, *J. gen. Viro,* 1986, **67**, 2135-2143.
2 R.K. Madan, J. Levitt, *J Am Acad Dermatol*, 2014;70:788-92.
3 P.E. Grimes, MD, *Dermatol surg,* 1999, **25**, 19.
4 W. Roberts, *Dermatologic Therapy*, 2004, **17**, 196–205.
5 P. Trinder, Branched *Chain Fatty acids of Butterfat,* 1953, **57**, 301-303
6 M.J. Gil and V.M. Merino, iupac.org/home/publications, 2007, **1**, 11
7 C.G. Kontoyannis, and M. Orkoufa, *Talanta* 1994, **41**, 1981-1984,
8 K. Kltamura and R. MaJima, Anal. Chem. 1983, **55**, 54-56.
9 C. Deng, X. Zhang, J. Zhang, J. Qian, W. Zhu, *Chromatographia*, 2003, **58**, 225.
10 N.A. Farid, G. S. Born, W.V. Kessler, S.M. Shaw, and W.E. Lange, *Clin. Chem*, 1975, **21**, 1167-1168.
11 X.Xu, L. Koetzner, J. Boulet, H. Maselli, J. Beyenhof and G. Grover, *Chromatogr*. 2009, **23,** 973–979.
12 S.K. Bae, K.A. Seo, E.J. Jung, H.S. Kim, C.W. Yeo, J.H. Shon, K.M. Park, K.H. Liu, and J.G. Shin, *Biomed.Chromatogr*. 2008, **22**, 590–595.
13 S.L. Ali, *Chromatograp*, 1973, **6**, 478.
14 W. De Zhang, B. Xu, Y.X. Hong, Y.X. Yu, J.S.Ye, J.Q. Zhang, *J Solid State Electrochem.,*2010, **14,** 1713–1718.
15 M.H.A. Zavar, S. Heydari, G.H. Rounaghi, *Arabian Journal for Science and Engineering*, 2013, **38**, 29-36.
16 T. Selvaraju, and R. Ramaraj, *J. Chem. Sci.* 2014, *126*, 11–16.
17 H. Yang, B. Lu, L. Guo, B. Qi, *J. Electroanal. Chem,* 2011, **650**, 171–175.
18 L. Qua, S. Yang, G. Li, R. Yang, J. Li, L. Yu, *Electrochim. Acta,* 2011, **56**, 2934–2940.

19 Y. Liu, Z. Yang, Y. Zhong, J. Yu, *Applied Surface Science*, 2010, **256**, 3148–3154.
20 Q. Sheng, H. Yu, J. Zheng, *J. Electroanalytical Chem.*, 2007, **606**, 39–46.
21 P. Wu, C. Cai, *Electroanalysis* 2005, **17**, 1583.
22 P. Wu, Y. Shi, C. Cai, *J Solid State Electrochem.*, 2006, **10**, 270–276.
23 P. Wu, S. Lu, C. Cai, *J. Electroanalytical Chem.*, 2004, **569**, 143–150.
24 P. Wu, C. Cai, *J Solid State Eletrochem*, 2004, **8,** 538–543.
25 A. Eftekhari, *Electroanalysis*, 2004, **16,** 1324.
26 L.D. Feng, M.Mi. Gu, Y.L. Yang, G.X. Liang, J.R. Zhang, and J.J. Zhu, *J. Phys. Chem. C.*, 2009, **113**, 8743–8749.
27 B. Fang, R. Shen, C. Zhang, H. Yuan, L. Yao, G. Wang, *Electroanalysis*, 2009, **21**, 2680 – 2684.
28 P. Wu, C. Cai, *Chinese Journal of Chemistry*, 2005, **23**, 127—131.
29 Y. Sun, W. Zhou, D. Zhao, J. Chen, X. Li, L. Feng, *Int. J. Electrochem. Sci.*, 2012, **7,** 7555 – 7566.
30 M. Rajkumar, B. Devadas, S.M. Chen, *Electrochimica Acta*, 2013, 105, 439– 446.
31 B. Devadas, H.T. Yeh, S.M. Chen, *Electroanalysis*, 2014, **26**, 1 – 10.
32 M.G. Martın, M.L.R. Mendez, and J.A.d. Saja, *Langmuir*, 2010, **26**, 19217–19224.
33 T.V. Magdesieva, K.P. Butin, T. Yamamoto, D.A. Tryk, and A. Fujishima, *J. Electrochemical Society*, 2003, **150**, E608-E612.
34 I. Yilmaza, T. Nakanishi, A. Gürek and K. M. Kadish, *J. Porphyrins Phthalocyanines*. 2003, **7,** 227-238.
35 S. Karadag , C. Bozoglu , M. K. Sener , A. Koca, *Dyes and Pigments*, 2014, **100,** 168-176.
36 C. Bozoglu, M. Arıcı, A. L. Ugur, A. Erdogmus¸ A. Koca, *Synthetic Metals*, 2014, **190,** 56–65.
37 F. Schedin, A.K. Geim, S.V. Morozov, E.W. Hill, P. Blake, M.I. Katsnelson, K.S. Novoselov, *Nature materials*. 2007, **6**, 652 - 655.
38 M.D. Stoller, S. Park, Y. Zhu, J. An, R.S. Ruof, Graphene-Based Ultracapacitors, *Nano Lett.*, 2008, **8,** 10.
39 B. Devadas, V. Mani, S.M. Chen, *Int. J. Electrochem. Sci.*, 2012, **7,** 8064 - 8075.
40 V. Mani, B. Devadas, S.M. Chen, *Biosensors and Bioelectronics*, 2013, **41,** 309–315.
41 Y. Shao, J. Wang, H. Wu, J. Liu, I. A. Aksay, Y. Lin, *Electroanalysis*, 2010, **22,** 1027 – 1036.
42 Nakamoto, K. John Wiley & Sons, Inc.: New York, 1986.
43 G. Zhao, J.J. Feng, Q.L. Zhang, S.P. Li, and H.Y. Chen, *Chem. Mater*. 2005, **17**, 3154-3159.
44 J. Yang, J. R. Stricklerb and S. Gunasekaran, *Nanoscale*, 2012 **4**, 4594-602.
45 M. A. Raj and S. A. John, *J. Phys. Chem. C*, 2013, **117**, 4326-35
46 P. Lu, S. Liu, G. Dai, Y. Lei and Y. Liang, *Australian Journal of Chemistry*, 2013, **66**, 983-988.
47 K. Subramani, D. Jeyakumar and M. Sathish, *Phys. Chem. Chem. Phys*, 2014, **16**, 4952-4961.
48 M. B. Gholivand, M. Khodadadian, and M. Omidi, *Materials Science and Engineering C*, 2013, **33**, 774–781.
49 B. Devadas, M. Rajkumar, S.M. Chen, R. Saraswathi, *Int. J. Electrochem. Sci*, 2012, **7**, 3339 – 3349.
50 L. P. Bicelli, B. Bozzini, C. Mele, L. DUrzo, *Int. J. Electrochem. Sci.*, 2008, **3**, 356 – 408.
51 C. Z. Zhu, S. J. Guo, Y. X. Fang and S. J. Dong, ACS Nano, 2010, **4**, 2429–2437.
52 D.M. Gil , M.C. Navarro, M.C. Lagarrigue, J. Guimpel , R.E. Carbonioc, M.I. Gomez, *Journal of Molecular Structure*, 2011, **1003**, 129–133.
53 M. Broschoa, M. Mihalik, V. Kavecansky, M. Seberini, W. Suski, *Czechoslovak Journal of Physics*, 2002, **52**, 325.
54 A.L. Oleksiak, A.P. Nowak, M. Wilamowska, M. Sikora, W. Szczerba, Cz. Kapusta, *Synthetic Metals*, 2010, **160**, 1234–1240.
55 T.R.I. Cataldi, G.E.D. Benedetto, A. Bianchini, *Journal of Electroanalytical Chemistry*, 1998, **448**, 111–117.
56 A.P. Grosvenor, B.A. Kobe, M.C. Biesinger and N.S. McIntyre, *Surf. Interface Anal*. 2004, **36,** 1564–1574.
57 C. Cofan and C. Radovan, *International Journal of Electrochemistry*, Volume 2011, Article ID 451830, 9 pages.
58 2. M. Yousef Elahi , S.Z. Bathaie, S.H. Kazemi, and M.F. Mousavi, *Anal. Biochem*. 2011, **411,** 176–184.
59 E. R. Sartori, R. A. Medeiros, R. C. R. Filho and O.F. Filho, J. *Braz. Chem. Soc*, 2009, **20,** 360-366.
60 D. P. Venema, P. C. H. Hollman, K. P. L. T. M. Janssen, and M. B. Katan, *J. Agric. Food Chem.* 1996, **44,** 1762−1767.
61 M. Doulache, A. Benchettara, and M. Trari, *Journal of Analytical Chemistry*, 2014, **69,** 51–56.
62 Z. Wang, F. Ai, Q. Xu, Q. Yang, J. H. Yub, W. H. Huang, Yuan-Di Zhao, *Coll. and Surfaces B: Biointerfaces*, 2010, **76,** 370–374.
63 I. Gualandi, E. Scavetta, S. Zappoli, D. Tonelli, *Biosensors and Bioelectronics*, 2011 **26,** 3200–3206.

Table 1 Comparison of analytical parameters for detection of SA over various modified electrodes

Modified electrodes[a]	Detection limit (μM)	Concentration range (μM)	Sensitivity (μA mM^{-1} cm^{-2})	Reference
Well-aligned MWCNTs	0.8	2–3000	59.25	14
BDD in sodium sulphate medium	1	10–100	24.17	57
DNA/PPy Nanofiber modified electrode	0.8	0.1–2	---	58
BDD	2	2.5–105	58.66	59
HPLC with Fluorescence detection	0.02 0.2 (mg/Kg)	---	---	60
Ni/GCE	0.5	2–550	63.78	61
PNP/Pt disk electrode	6.4	20–500	0.219	62
Co/Al hydrotalcite coated-Pt	6	10–500	---	63
LuHCF/RGO/GCE	0.49	5–1000	77.2	This work

[a] MWCNTs – Multiwalled carbon nanotube; BDD – Boron-Doped Diamond Electrode; PPy – polypyrrole; PNR – platinum nanoparticles; Ni – Nickel modified GCE; Co/Al – cobalt hydrotalcite-like.

Journal Name RSCPublishing

ARTICLE

Table 2. Performance of LuHCF/RGO/GCE for the determination of Salicylic acid (SA) in real samples.

S. No	Tablet sample	Added (μM)	Found (μM)	Recovery %
1	Sample 1	200	199.45	99.7
2	Sample 2	400	377.26	94.3
3	Sample 3	700	692.72	98.96